Photosystem trap energies and spectrally-dependent energy-storage efficiencies in the Chl d-utilizing cyanobacterium, Acaryochloris marina

4 authors, including:

Some of the authors of this publication are also working on these related projects:

Project   Dynamically Superhelical DNA View project

Project   Native Masspec View project

Photosystem trap energies and spectrally-dependent energy-storage efficiencies in the Chl *d*-utilizing cyanobacterium, *Acaryochloris marina*

Steven P. Mielke [a,*], Nancy Y. Kiang [b], Robert E. Blankenship [c], David Mauzerall [a]

[a] *Laboratory of Photobiology, The Rockefeller University, New York, NY 10065, USA*
[b] *NASA Goddard Institute for Space Studies, New York, NY 10025, USA*
[c] *Departments of Biology and Chemistry, Washington University in St. Louis, St. Louis, MO 63130, USA*

ABSTRACT

Acaryochloris marina is the only species known to utilize chlorophyll (Chl) *d* as a principal photopigment. The peak absorption wavelength of Chl *d* is redshifted ≈ 40 nm *in vivo* relative to Chl *a*, enabling this cyanobacterium to perform oxygenic phototrophy in niche environments enhanced in far-red light. We present measurements of the *in vivo* energy-storage (E-S) efficiency of photosynthesis in *A. marina*, obtained using pulsed photoacoustics (PA) over a 90-nm range of excitation wavelengths in the red and far-red. Together with modeling results, these measurements provide the first direct observation of the trap energies of PSI and PSII, and also the photosystem-specific contributions to the total E-S efficiency. We find the maximum observed efficiency in *A. marina* ($40 \pm 1\%$ at 735 nm) is higher than in the Chl *a* cyanobacterium *Synechococcus leopoliensis* ($35 \pm 1\%$ at 690 nm). The efficiency at peak absorption wavelength is also higher in *A. marina* ($36 \pm 1\%$ at 710 nm *vs.* $31 \pm 1\%$ at 670 nm). In both species, the trap efficiencies are $\approx 40\%$ (PSI) and $\approx 30\%$ (PSII). The PSI trap in *A. marina* is found to lie at 740 ± 5 nm, in agreement with the value inferred from spectroscopic methods. The best fit of the model to the PA data identifies the PSII trap at 723 ± 3 nm, supporting the view that the primary electron-donor is Chl *d*, probably at the accessory (Chl_{D1}) site. A decrease in efficiency beyond the trap wavelength, consistent with uphill energy transfer, is clearly observed and fit by the model. These results demonstrate that the E-S efficiency in *A. marina* is not thermodynamically limited, suggesting that oxygenic photosynthesis is viable in even redder light environments.

© 2012 Elsevier B.V. All rights reserved.

1. Introduction

The principal photopigment in nearly all known oxygenic phototrophs is chlorophyll (Chl) *a*. The unique properties of Chl *a* have made it all but indispensable to O$_2$-producing photosynthesis, both as a light harvesting pigment, and as a redox cofactor central to primary photochemistry [1–3]. In particular, within the reaction center (RC) of Photosystem II (PSII), Chl *a* generates a standard-state oxidation potential of $\approx +1.2$ V—the highest in any known biological system—and thereby mediates the energetically formidable reaction that extracts four electrons from water, releasing molecular oxygen.

Recently discovered cyanobacteria that contain novel chlorophylls Chl *d* and Chl *f* have demonstrated that exclusive use of Chl *a* is not a universal requirement of oxygenic photosynthesis. These organisms are found in niche environments enhanced in far-red/near-infrared light, where they have adapted by employing long wavelength-absorbing chlorophylls in oxygenic phototrophy [4]. The red-shifted absorption of these pigments extends the spectral range for oxygenic photosynthesis, previously assumed to be limited to wavelengths shorter than 700 nm, increasing the available photon flux by as much as 20% [5]. These cyanobacteria include the Chl *d*-dominated *Acaryochloris marina* [4,6–8], the recently characterized, Chl *f*-containing *H. hongdechloris* [5,9,10], and an *Acaryochloris*-like symbiont, *Candidatus Acaryochloris bahamiensis*, inhabiting shallow-water marine ascidians in the Bahamas [11].

In *A. marina*, Chl *d* comprises > 95% of the total chlorophyll content [6], and functions as both a light harvesting pigment and an RC cofactor [12]. Chl *d* results from a vinyl→formyl substitution at the C3 position on ring A in Chl *a*. This shifts the Q$_Y$ absorption maximum by ≈ 30 nm *in vitro* (from 665 nm for Chl *a* to 696 nm for Chl *d* in methanol) [5] and by ≈ 40 nm *in vivo* [6]. The *in vitro* oxidation potential of Chl *d* is $+0.88$ V *vs.* $+0.81$ V in Chl *a* [13].

There is consensus that the primary electron donor of Photosystem I (PSI) in *A. marina* is a Chl *d* dimer; however, the possibility

that the primary acceptor (A_0) is Chl a has not been ruled out [12,14]. Similarly, there is consensus that Chl d has replaced Chl a at the Chl_{D1}, Chl_{D2}, and P_{D2} sites in PSII, but debate remains on whether P_{D1}, the active-branch special-pair chlorophyll, is Chl d or a [12,15–20]. Depending on the identity of the trapping chlorophyll, excitation of the PSII RC in $A. marina$ may require thermodynamically uphill energy transfer from longer wavelength-absorbing antenna complexes. Even if transfer to the RC is predominantly downhill, a lower initial energy of the excited Chl d trap may require primary photochemistry that is energetically uphill. Thus, despite the potential for increased light-harvesting efficiency, the need for uphill energy transfer may compromise the energy-storage (E-S) efficiency by limiting the quantum yield. Therefore, determining the E-S efficiency in $A. marina$ and other far-red organisms, relative to that in Chl a-utilizing species, directly addresses the long-wavelength limit of oxygenic photosynthesis, and will potentially identify mechanisms that extend this limit, as well as factors that fundamentally constrain those mechanisms.

The word 'efficiency' has many meanings in the context of photosynthesis [21,22]. Here, we intend it to mean the maximal energy-storage efficiency of the system; $i.e.$, the percentage of monochromatic photon energy that is stored as enthalpy when the pulse energy is extrapolated to zero to remove saturation effects: $\varepsilon_{max} \equiv \lim_{E_{abs} \to 0} \varepsilon$, where

$$\varepsilon \equiv E_{sto}/E_{abs} = (E_{abs} - E_{dis})/E_{abs}. \tag{1}$$

At a chosen wavelength and laser flash energy, E_{sto} is the energy stored by the photosynthetic sample, E_{abs} is the energy absorbed, and E_{dis} is the energy dissipated as heat following excitation, which is detected by PA measurement. Under non-saturating conditions, some of the excitation (absorbed pulse) energy is retained by the sample as a consequence of photochemistry ($i.e.$, $E_{dis} < E_{abs}$); thus, $E_{abs} - E_{dis} = E_{sto}$ as a fraction of E_{abs} gives the energy-storage efficiency, ε. Extrapolation to zero-energy of measurements of ε over a range of pulse energies then gives ε_{max} (Sections 2.2 and 3.1).

There has been a vast amount of work on the kinetics and reaction center structures of photosynthetic systems. Far less work has been done on the thermodynamics of these systems. The development of pulsed, time-resolved photoacoustic (PA) methodology has allowed the direct measure of the enthalpy of photochemical reactions, and thus of the efficiency of photosynthesis [23–25]. The very difficult problem of determining the light absorbed by these complex, light-scattering systems, and the laborious estimation of the products, are replaced by (in principle) two microsecond laser flashes and recording of the produced sound waves. Our previous PA measurements [26] have shown that the millisecond-timescale E-S efficiency in whole cells of $A. marina$ ($\varepsilon_{max} \approx 40\%$) is comparable to or even higher than that of typical oxygenic species at the wavelength of maximum Chl absorption ($\approx 34\%$ in the Chl a cyanobacterium $Synechococcus\ leopoliensis$ and $\approx 43\%$ in the alga $Chlorella\ vulgaris$ [27]). The study reported in Ref. [26] used single experimental wavelengths, chosen to be at the peak light absorption of the Chl Q_Y band; $i.e.$, 710 nm in $A. marina$ and 670 nm in $S. leopoliensis$. At these wavelengths, in whole cells, both PSI and PSII contribute to photosynthesis in the natural context, allowing determination of the overall efficiency of $in\ vivo$ energy storage. However, because it excited the systems at only one wavelength, the Ref. [26] study did not provide the individual contributions of PSI and PSII to the total efficiency. This and other photosystem-specific information, such as the trap energy, can be obtained by measuring the E-S efficiency at excitation wavelengths spanning the photochemically relevant spectral range.

In this paper we expand our PA study of energy storage in $A. marina$ to wavelengths between 670 and 760 nm (measurements at 5 nm intervals), and obtain the $in\ vivo$ E-S efficiency as a function of the wavelength. These measurements are of unprecedented wavelength resolution (1 nm) and accuracy in the efficiency (99%). This allows us to present a model for determining the absolute trap energies and relative contributions of the photosystems to the observed energy storage. We also discuss the decrease in efficiency and role of uphill energy-transfer in the spectral regions to the red of the photosystem traps.

2. Materials and methods

2.1. Cell growth and sample preparation

$A. marina$, strain MBIC11017 (obtained from the Blankenship Lab, Washington University, St. Louis), was grown in MBG-11 medium at 28 °C with continuous agitation (100 rpm) [4]. Continuous light was provided by an incandescent bulb at an average intensity of 15 µE m^{-2} s^{-1} of photosynthetically active radiation (PAR). $S. leopoliensis$ (UTEX 625) was grown in Allen's or BG-11 medium at 21 °C with continuous agitation (100 rpm). Continuous light was provided by four fluorescent bulbs at an average intensity of 50 µE m^{-2} s^{-1} PAR. For both $A. marina$ and $S. leopoliensis$, log phase cells containing 3–7 µg chlorophyll ml^{-1} medium were affixed under mild vacuum to filters (HAWP04700, 0.45 µm pore size, Millipore) cut to 1.4 cm diameter. 1 ml medium containing 3 mM NaHCO$_3$ was added to 1 ml cell culture for filtration, yielding samples for which photoacoustic signals were both reproducible and proportional to laser energy. Filters were pre-washed with 5 ml pure 70% ethanol and rinsed with distilled water. Filtration was stopped prior to the liquid level being drawn off the filter, so that samples remained wet while transferred to the sealed PA cell (see below). For measurements at excitation wavelengths where sample absorption was low, larger (up to 3×) cell volumes were used to maintain signal-to-noise ratio (Section 2.2). Absorbance spectra (see Fig. 3) of entire samples (cells and bicarbonate medium on filters) were obtained using an Olis spectrophotometer (model DW2A conversion) with resolution 1.5 nm. Blank control filters were prepared in the same way as the samples; $i.e.$, pre-washed with ethanol and rinsed, then washed with 1 ml medium + 1 ml 3 mM NaHCO$_3$ under vacuum.

2.2. Millisecond-timescale photoacoustic (PA) measurements in vivo

The PA cell is the same as that described in Ref. [28]. Samples were illuminated at selected wavelengths using an Optical Parametric Oscillator (OPO) (Uniwave Technology) pumped by a 532 nm flashlamp-pumped Nd:YAG laser (Surelite II, Continuum) with 7-ns pulses at a frequency of 3.3 Hz. The YAG laser was tuned to minimum pulse width (7 ns) and delay time. Tuning to maximum power can result in low efficiency in the OPO. The OPO output, after removal of green light, was attenuated in steps by neutral density filters. Pulse wavelength and purity were measured using an SD2000 spectrometer (Ocean Optics). The full width at half-maximum intensity of the pulses was < 1 nm (the resolution of the instrument). The wavelength range of the experiments (670 nm ≤ λ_{ex} ≤ 760 nm) was determined at short wavelength by the physical range of the OPO and at long wavelength by the background absorption of the samples. At all wavelengths the samples were optically thin, peak absorbance ≈ 0.1. The limiting long wavelength occurs when the sample signal approaches that of the filter background. The maximum excitation wavelength used (725 nm for $S. leopoliensis$ and 760 nm for $A. marina$) was the longest with adequate signal.

Light pulses were led to the dark-adapted sample via a liquid light guide (S2000, Newport). Output from the PA microphone was wired to a high impedance, low noise amplifier (Ithaco model 1201, filters 3 and 300 Hz, gain ×100) and thence to a Tektronix TDS540 digital oscilloscope to record and average the pulses. The pulse number varied from 30 to 400 depending on the S/N of the measurement. The averaged data were read into a computer along with the averaged light pulse energy obtained by a calibrated pick-off and a Coherent model EPM 2000 light detector. Data were collected and analyzed using MATLAB [29] programs written by SPM. The computer opened

a shutter for the light pulses, collected data, then closed the shutter on completion.

Saturating continuous light with IR removed was applied to the sample *via* a light guide from a Cole Parmer model 9741-50 illuminator, and the measurement sequence repeated. The continuous light was set at 35 W by DC power supply (GPR-1810HD, GWInstek), sufficient to saturate but not heat the samples. The sample was changed after each saturating illumination so as not to wait for the recovery time. Since the efficiency is calculated from the ratio of the dark to light signal maxima from the same sample (see below), small variations of cell or water content between samples do not affect the results. A small (0.05 mV/µJ) contribution from the filter substrate, measured using blank control filters, was subtracted from all measured signals. At low ($< \approx 10$ µJ/cm^2) flash energies, the efficiency decreases linearly with increasing energy [28], allowing ε_{max} to be calculated by extrapolation to zero energy with a linear fit to a set of low-energy data [26,27,30] (see Fig. 1 and Section 3.1). At each experimental wavelength, ε_{max} was calculated from a dataset consisting of PA measurements from several culture batches, and thus inherently reflects the average batch-to-batch variation of the efficiency (Fig. 1).

The signal obtained from a PA measurement is the rate of pressure change, dP/dt, not the pressure itself [28]. Integrals of the PA signals, $P(t)$, can also be used to obtain efficiencies. (Since the system is linear, both dP/dt and P are proportional to the energy.) The E-S efficiency at a chosen flash energy and wavelength was calculated from the signal maxima (*e.g.*, Fig. 2 in Ref. [26]). The maximum in dP/dt occurs at an early time following the flash, ≈ 3 ms. This is ideal because the PA

cell is not thermostated. Thus, any change in room temperature affects the rate of cooling from the heat of the flash (≈ 2–20 milli°), which occurs on the 10–50-ms timescale. Because this manifests itself as a drift in the PA signal baseline, the shorter the time from the baseline measure before the flash to the time of measurement, the lesser the error. Therefore, the short time (≈ 3 ms) to the signal maximum gave the most reliable results. The 3 Hz rate of excitation allowed time for cooling between pulses when the data were averaged.

The energy stored is affected by the rate and length of excitation. In the ideal case of limiting zero-energy excitation, the products would be the S-states S1 or S2 (depending on the population of the dark-adapted state) and Q_B^- for PSII, and ferredoxin or FAD$^-$ and PQ for PSI, since only one electron would be moved. In actuality, with our 100–400 weak pulses, the products are O_2 and NADPH (Sections 3.1 and 4.1). This is because the weak excitation scores only 0.01 to 0.1 hits per pulse (1–10-µJ pulse and effective optical cross-section $\sigma \approx 0.0086$/µJ at the peak absorption); however, with 100–400 pulses all the units are excited at least once. A good approximation is obtained from the total pulse energy, since the pulses are independent and we assume no changes in the antenna complexes. The total energy is then 400–1000 µJ and the average hits are 5–12 (with $\sigma = 0.0086$/µJ). Thus 56% of the systems have been hit 5 or more times (and 54% 12 or more times), and are well on their way to final products. Since we see no excess loss of efficiency at the lowest energy compared to that at ten-fold higher energy (Section 3.1), the progress of the S-states seems to have no effect. This is in agreement with claims that the enthalpy changes of the S-states are all the same (*e.g.*, [31]; Mauzerall, unpublished data). Similarly, possible loss of the S3 state because of long delay between hits will have little effect (at 0.01 hits per pulse, the time for complete re-excitation is about 30 s, approaching the lifetime of S3).

2.3. Model of energy-storage (E-S) efficiency vs. excitation wavelength

The spectral dependence of the observed efficiencies is determined by that of the underlying contributions to energy storage specific to PSI and PSII. These contributions are in turn determined by the respective trap energies. To obtain these photosystem-specific efficiencies and energies, we have developed a novel modeling procedure for fitting the unprecedented PA spectral efficiency data. The fractional contributions of the photosystems are determined from sample absorbance data and available information on specific PSI and PSII pigment bands. For each photosystem, the efficiency is assumed to (1) increase proportionally with the excitation wavelength for wavelengths shorter than that of the trap, accommodating fast downhill energy-transfer losses; and (2) decrease as a function of an exponential factor with increasing wavelength for wavelengths longer than that of the trap, accommodating thermally-activated uphill energy transfer. See Sections 3.3 and 4.3 for modeling results and discussion. Further details of the procedure are provided in the Appendix.

3. Results

3.1. E-S efficiencies from in vivo PA

Results of PA measurements of the ms-timescale E-S efficiency of *A. marina* (*Am*) and *S. leopoliensis* (*Sl*) whole cells are shown in Fig. 1A and B, respectively. Measurements were obtained in *Am* at 710 nm with flash energies between 2 and 11 µJ, and in *Sl* at 670 nm with flash energies between 2 and 13 µJ. These energies are sufficiently low that multiple hits were negligible, and a linear correlation could be made to obtain the ideal, zero absorbed-energy efficiency, ε_{max} (Section 2.2). For *A. marina* $\varepsilon_{max,710\ nm} = 36 \pm 1\%$, and for *S. leopoliensis* $\varepsilon_{max,670\ nm} = 31 \pm 1\%$ (*cf.*, corresponding data points in Fig. 2).
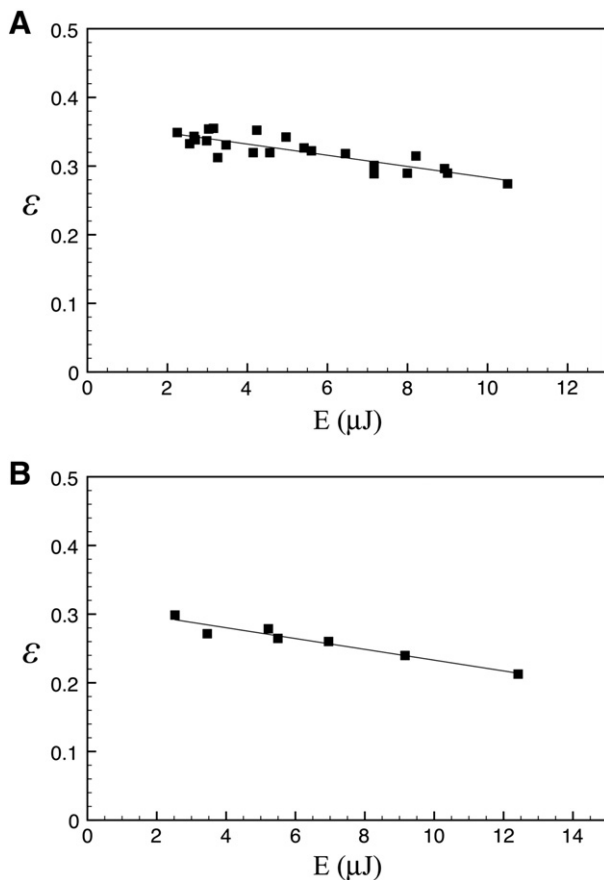
Fig. 1. E-S efficiency (ε) *vs.* laser pulse energy incident on samples containing (A) *A. marina* intact cells (pulse wavelength $\lambda = 710$ nm); and (B) *S. leopoliensis* intact cells ($\lambda = 670$ nm). Energies are per 1.5 cm^2 sample area. The *Am* data were obtained from three different cell cultures. The maximum efficiency, ε_{max}, is obtained from the y-intercept of a linear fit to the data. Here, $\varepsilon_{max} = 36 \pm 1\%$ (*Am*) and $31 \pm 0.7\%$ (*Sl*).

Fig. 2. Maximal E-S efficiency ($\varepsilon_{\max}$) *vs.* wavelength (λ) in *A. marina* (filled circles) and *S. leopoliensis* (open circles) whole cells. Error bars indicate the RMS deviation of the linear fit corresponding to each data point (*cf.*, Fig. 1). Fits of the expected total efficiency (Eq. (A.3)) to the data, incorporating three (solid curve) or six (dashed curve) Gaussian absorption bands in *A. marina*, and three bands (dotted curve) in *S. leopoliensis*, are shown. Abso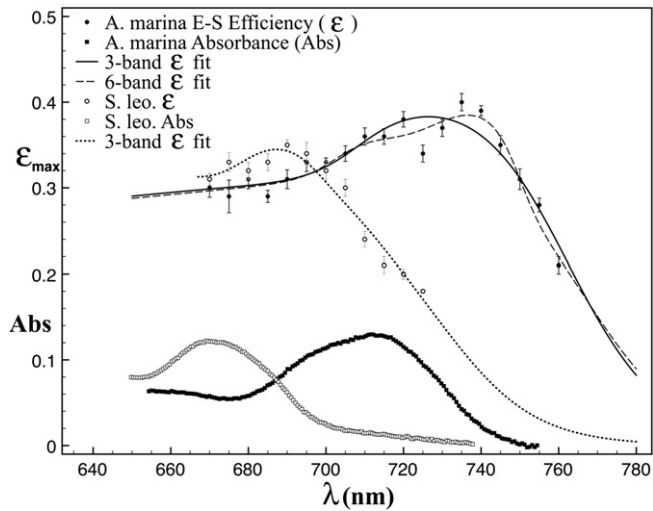rbance data obtained from the PA samples (filled and open squares) are shown here for reference, and are reproduced in Fig. 3.

3.2. Spectral dependence of the in vivo efficiency

Repeating this procedure at 5-nm intervals between 670 and 760 nm (*Am*) and between 670 and 725 nm (*Sl*), we obtained $\varepsilon_{\max}$ as a function of pulse wavelength in both cyanobacteria. The resulting efficiency spectra are shown in Fig. 2, where filled circles and squares are maximum E-S efficiencies [$\varepsilon_{\max}(\lambda)$] and measured absorbances [Abs(λ)] of *A. marina* intact-cell samples, and open circles and squares are $\varepsilon_{\max}(\lambda)$ and Abs(λ) of *S. leopoliensis* samples. In *Am*, the efficiency rises from $30 \pm 1\%$ at 670 nm to $38 \pm 0.9\%$ at 720 nm, falls to $34 \pm 1\%$ at 725 nm, rises again to $40 \pm 1\%$ at 735 nm, then decreases with increasing wavelength to $21 \pm 1\%$ at 760 nm. In *Sl*, $\varepsilon_{\max}$ rises from $31 \pm 0.7\%$ at 670 nm to $35 \pm 0.6\%$ at 690 nm, then decreases with increasing wavelength to $18 \pm 0.2\%$ at 725 nm. The highest efficiency in either species is therefore that in *Am* at 735 nm.

3.3. Analysis of the spectral efficiency

3.3.1. Fractional contributions to energy storage from sample absorbance

Modeling $\varepsilon_{\max}(\lambda)$ in *Am* and *Sl* (Section 2.3, Appendix) required first determining the fractional contributions to energy storage specific to PSI and PSII; *i.e.*, $F_{I,II}$ in the model expression for the observed efficiency (see Eqs. (A.1)–(A.3)). Results of fitting Gaussian bands to *Am* and *Sl* absorbance data to obtain these contributions (see Eqs. (A.4)–(A.8)) are as follows.

3.3.1.1. A. marina (3 or 6 absorption bands).
The fit of three PSI and PSII bands (Eq. (A.5) + Eq. (A.6)) to the *A. marina* data (Fig. 3A, solid curve through filled circles) yields final parameter values (Table 1, Column 1) that agree with previous intact-cell studies; for example, Schiller et al. [32] identified absorption bands associated with phycobilins near 650 nm, and bands associated with Chl *d* near 695, 715, 728, and 741 nm at low temperature (77 K). The bands at 728 and 741 nm are evident at 77 K, but are not resolved at room temperature (Figs. 1 and 2 in Ref. [32]). The root-mean-square error (RMSE) of this fit is ≈ 0.001, or 1% of the absorbance.

The parameter values from the fit of six bands [Eq. (A.7) + Eq. (A.8)] to the *A. marina* data (Fig. 3A, dotted curve through filled circles) are shown in Table 1, Column 2. Note that the bandwidths are as expected:
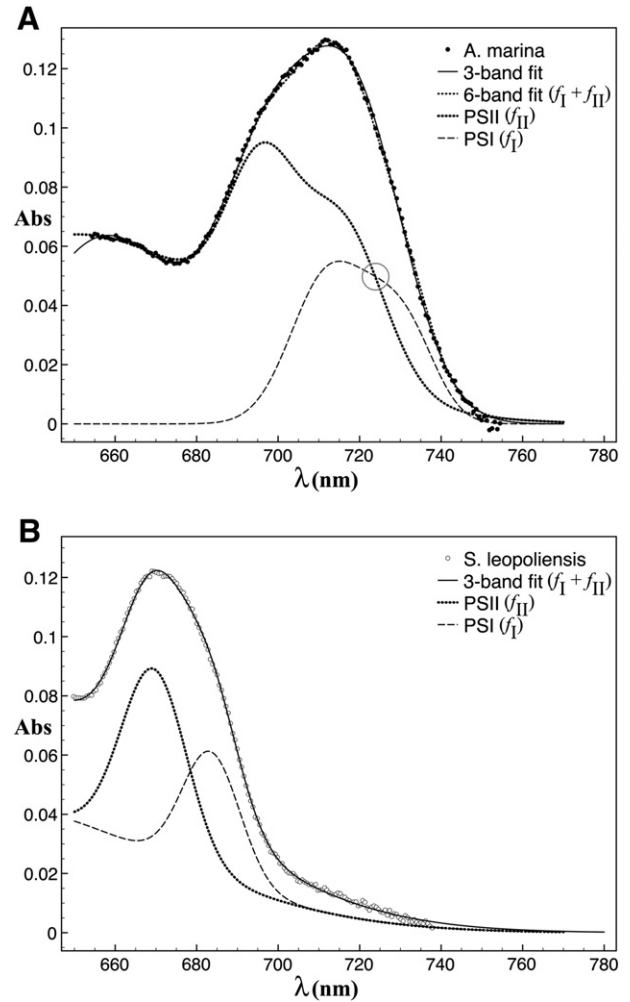

Fig. 3. (A) Filled circles are the absolute absorbance of a PA sample consisting of *A. marina* whole cells on filter paper (Section 2.1). The solid and dotted curves through the data are fits of the combined Gaussian absorbances of PSI and PSII, $f_I + f_{II}$; *i.e.*, [Eq. (A.5) + Eq. (A.6)] (three bands) and [Eq. (A.7) + Eq. (A.8)] (six bands), respectively (see Appendix A and Table 1). The smaller dashed and dotted curves are the separate components f_I and f_{II} of the six-band fit, with the phycobilin contribution $p_I = 0$ (Sections 3.3.2 and Appendix). The crossing of f_I and f_{II} near 725 nm (gray circle) coincides with an apparent dip in the observed efficiency, approximately captured by the model when $f_{I,II}$ is determined by six bands (dashed curve in Fig. 2). (B) Absolute absorbance of a sample consisting of *S. leopoliensis* whole cells. The solid curve through the data is the fit of $f_I + f_{II}$ (three bands; see Table 1). The dashed and dotted curves are the PSI and PSII components f_I and f_{II}, with $p_I = 0.5$.

$\approx 10 \pm 2$ nm for the Chl bands and much broader for the phycobilin bands. The RMSE of this fit is ≈ 0.001.

3.3.1.2. S. leopoliensis (3 absorption bands).
The fit of three bands to the *S. leopoliensis* data (Fig. 3B, solid curve through open circles) yields parameter values (Table 1, Column 3) that agree with bands identified by previous intact-cell and isolated-photosystem studies of *Synechococcus* spp. and other Chl *a* cyanobacteria [5,33–35]. The RMSE of this fit is ≈ 0.001.

3.3.2. Trap energies and E-S efficiencies from PA data

Using $F_{I,II}$ as determined above, and following the procedure detailed in the Appendix, the model expression Eq. (A.3) was fit to the spectral efficiency data to obtain the wavelengths ($\lambda_{t;I,II}$) and efficiencies ($\varepsilon_{t;I,II}$) specific to the PSI and PSII traps. The results are as follows.

3.3.2.1. A. marina (3 or 6 absorption bands).
Results of fitting to the *A. marina* efficiency data assuming three or six absorption bands

Table 1
Final parameter values from fits of the combined PSI and PSII absorption to *A. marina* or *S. leopoliensis* absorbance data (Fig. 3). For each pigment band, the parameters are the Gaussian amplitude, peak location, and half-width. Column 1 and 3 values were obtained by fitting three bands (Eq. (A.5) + Eq. (A.6)) and Column 2 values by fitting six bands (Eq. (A.7) + Eq. (A.8)). The three-band fits were performed by non-linear least squares, and the six-band fit by inspection such that the root-mean-square error (RMSE) was minimized. Uncertainties in fitted values of the parameters are indicated (95% confidence bounds). The RMS errors of all three fits are shown.

Parameters	*A. marina*		*S. leopoliensis*
	3-band[a]	6-band[b]	3-band[c]
A	0.11 ± 0.01	0.049	0.042 ± 0.006
B (nm)	718.5 ± 1	712	683.5 ± 0.9
C (nm)	12.2 ± 0.5	9.0	7.11 ± 0.4
D	0.063 ± 0.001	0.064	0.087 ± 0.01
E (nm)	657.9 ± 1	651	626 ± 7
F (nm)	18.26 ± 3	39	44.48 ± 3
G	0.079 ± 0.01	0.055	0.062 ± 0.004
H (nm)	697.0 ± 1	696	669.5 ± 0.8
I (nm)	11.7 ± 1	8.5	7.99 ± 0.4
J	–	0.032	–
K (nm)	–	728	–
L (nm)	–	8.0	–
M	–	0.007	–
N (nm)	–	735	–
O (nm)	–	6.0	–
P	–	0.052	–
Q (nm)	–	716	–
R (nm)	–	10	–

[a] RMSE = 0.0012.
[b] RMSE = 0.0010.
[c] RMSE = 0.00078.

(solid and dashed curves in Fig. 2) are shown in Table 2, Columns 1 and 2. The best fit incorporating three bands [Eqs. (A.5) and (A.6) with Gaussian parameters fixed at values in Table 1, Column 1] yields: $\lambda_{t,II} = 711 \pm 24$ nm, $\varepsilon_{t,I} = 0.41 \pm 0.02$, and $\varepsilon_{t,II} = 0.32 \pm 0.02$ (RMSE 0.017, 95% confidence bounds). The value and uncertainty of $\lambda_{t,I}$ (740 ± 5 nm) were obtained from the data as described in the Appendix. The procedures for determining the parameters $r_{I,II}^{-1}$ and p_I—*i.e.*, the photosystem-specific ratios of rate constants for primary separation, and the fractional contribution of phycobilins to PSI storage— are also described in the Appendix. Values of r_I^{-1}, r_{II}^{-1}, and p_I yielding the best fit with three bands are 0.14 ± 0.03, 0.14 ± 0.2, and 0 ± 0.4, respectively. $\lambda_{t,II}$, $r_{I,II}^{-1}$, and p_I are not well-defined by this fit.

The best fit to the *Am* data incorporating six bands [Eqs. (A.7) and (A.8) with parameters fixed at values in Table 1, Column 2] yields: $\lambda_{t,II} = 723 \pm 3$ nm, $\varepsilon_{t,I} = 0.43 \pm 0.02$, $\varepsilon_{t,II} = 0.32 \pm 0.01$ (RMSE 0.013, 95% confidence bounds). Values of $\lambda_{t,I}$, r_I^{-1}, r_{II}^{-1}, and p_I yielding the best fit with six bands are 740 ± 5 nm, 0.02 ± 0.05, 0.02 ± 0.01,

Table 2
Parameter values from fits of Eq. (A.3) to *A. marina* or *S. leopoliensis* efficiency data (Fig. 2). Uncertainties in parentheses were obtained either directly from the data ($\lambda_{t,I}$) or by refitting with the corresponding parameter (r_I^{-1}, r_{II}^{-1}, or p_I) free, and the remaining parameters fixed at the values shown.

Parameters	*A. marina*		*S. leopoliensis*
	3-band[a]	6-band[b]	3-band[c]
$\lambda_{t,I}$ (nm): PSI trap wavelength	740 (± 5)	740 (± 5)	695 (± 10)
$\lambda_{t,II}$ (nm): PSII trap wavelength	711 ± 24	723 ± 3	671 ± 6
$\varepsilon_{t,I}$: PSI trap efficiency	0.41 ± 0.02	0.43 ± 0.02	0.38 ± 0.04
$\varepsilon_{t,II}$: PSII trap efficiency	0.32 ± 0.02	0.32 ± 0.01	0.30 ± 0.05
r_I^{-1}: PSI rate constant ratio	0.14 (± 0.03)	0.02 (± 0.05)	0.02 (± 0.01)
r_{II}^{-1}: PSII rate constant ratio	0.14 (± 0.2)	0.02 (± 0.01)	0.02 (± 0.01)
p_I: fractional phycobilin contribution to PSI	0 (± 0.4)	0 (± 0.08)	0.5 (± 0.06)

[a] RMSE = 0.017.
[b] RMSE = 0.013.
[c] RMSE = 0.014.

and 0 ± 0.08. Including additional absorption bands improves both the RMSE and uncertainties of the fit.

3.3.2.2. S. leopoliensis (3 absorption bands). Results of the best fit to the *S. leopoliensis* efficiency data (dotted curve in Fig. 2) are shown in Table 2, Column 3. This fit yields: $\lambda_{t,II} = 671 \pm 6$ nm, $\varepsilon_{t,I} = 0.38 \pm 0.04$, and $\varepsilon_{t,II} = 0.30 \pm 0.05$ (RMSE 0.014, 95% confidence bounds). Values of $\lambda_{t,I}$, r_I^{-1}, r_{II}^{-1}, and p_I yielding the best fit are 695 ± 10 nm, 0.02 ± 0.01, 0.02 ± 0.01, and 0.5 ± 0.06.

4. Discussion

The present results most closely resemble the "action spectra" of research on photosynthesis. However, they differ in several basic features. First, they are absolute, measuring the total energy storage rather than the yield of a particular product of the different reaction systems. Thus, both photosystems are included, whereas measurements of oxygen or fluorescence changes provide information exclusively on PSII. Second, the present measurements are on whole cells under viable conditions. There is no damage or disruption of the systems or their interconnections by detergents and cell breakage. Third, since the energy is directly measured, the thermodynamic efficiency of the system is immediately available. Finally, because of the high energy-resolution (0.002 eV) and accuracy (99%) of the measurements, detailed analysis produces specific information on the separate photosystems. In the following, we will clarify these statements and explain the results of this work.

4.1. Efficiency at peak absorption wavelength vs. standard-state estimates

The $\approx$ 3-ms measurements reported here capture nearly complete photosynthesis, including O_2 formation [36] and electron transport almost to NADPH. Thus, all significant steps of the photosynthetic process are captured. The *in vitro* studies reported in Ref. [37] (also P. Sétif, personal communication) suggest $NADP^+$ reduction may require ~10 ms, indicating energy storage in reduced ferredoxin (Fd_{red}), and/or semi-quinone or fully-reduced ferredoxin-$NADP^+$ reductase (FNR_{sq} or FNR_{red}). We note that PA measures the total energy stored, not only that in the products. The enthalpy and entropy stored in proton gradients, protein conformations, and products of cyclic electron flow are all included.

At 710 nm in *Am* and 670 nm in *Sl* (absorbance maxima in Fig. 3) it is assumed the PA measurements capture approximately the overall efficiency of the two photosystem-mediated reaction:

$$2H_2O + 2NADP^+ \rightarrow 2NADPH + 2H^+ + O_2. \quad (2)$$
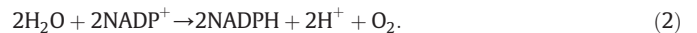
The present values of ε_{max} at 710 nm in *Am* and 670 nm in *Sl* ($36 \pm 1\%$ and $31 \pm 0.7\%$, respectively) differ slightly from those reported in Ref. [26], where small overcorrection for contributions to the PA signals from the sample substrate, in combination with batch variation, yielded somewhat higher values ($40 \pm 1\%$ and $34 \pm 1\%$, respectively). The present results are in closer agreement with the estimated efficiency of Reaction (2) [21,26]. In Ref. [26], the efficiency was estimated from standard-state midpoint redox potential differences as the energy stored per eight photons, assuming (a) each pair of photons excites PSII and PSI at the corresponding trap energy; (b) all excitations lead to primary charge separation (unity quantum yield); and (c) all charge-separated states reduce $NADP^+$ (no back- or side-reactions). This calculation also assumes that changes in entropy are negligible, equating enthalpy and free energy. In Chl *a* species, assuming excitation per two photons at 1.83 eV (680 nm) and 1.77 eV (700 nm) for PSII and PSI, respectively, and assuming a 1.14 V potential difference for Reaction (2) [26,38], the efficiency is estimated to be $\approx 32\%$. In *A. marina*, assuming excitation per two photons at 1.74 eV (713 nm) and 1.68 eV (740 nm) for PSII and

PSI, the efficiency is estimated to be $\approx 33\%$. Thus, energy storage in *A. marina* is expected to be more efficient if it produces the same final products as Chl *a* species using less trapped energy.

The efficiencies observed at 710 nm (*Am*) and 670 nm (*Sl*) in Fig. 2 are in close agreement with these estimates, with the observed efficiency in *Am* slightly higher than estimated (36% *vs.* 33%). Modes of energy storage that potentially elevate the measured efficiency with respect to the estimate include formation of a proton gradient [21,38]. The observed efficiency might also be higher than estimated if on the timescale of measurement the final products are predominantly Fd_{red}, FNR_{sq}, or FNR_{red} [37]. Even if the *in vivo* turnover time for NADPH production is faster than the *in vitro* times reported in Ref. [37], ε_{obs} might be higher in *A. marina* if its reaction kinetics differ from those in Chl *a* species. Quantification of the precise contributions to overall storage requires further investigation, while the results here may provide upper bounds.

Because they equate $\Delta G°$ *in vitro* with $\Delta G°$ *in vivo*, and assume $\Delta G° = \Delta H°$, efficiency estimates from standard-state potentials should be invoked with caution. To illustrate this, the above calculation applied strictly to PSI for the free-energy gap between PQ ($+0.1$ V [39]) and $NADP^+$ (-0.324 V [38]) predicts for 740-nm photons an efficiency of $\approx 25\%$. Applied to PSII for the gap between H_2O ($+0.816$ V [38]) and PQ, it predicts for 713-nm photons an efficiency of $\approx 41\%$. The former calculation significantly underestimates, and the latter overestimates, the efficiencies observed at these wavelengths (Fig. 2), as well as those predicted for the PSI and PSII traps by the model (Sections 3.3.2 [Table 2] and 4.3.4). Although the estimated total efficiencies agree with the PA measurements, the photosystem-specific estimates evidently miss essential elements of energy storage. These issues will be further addressed in a forthcoming article [40].

4.2. Three spectral regimes of the observed efficiency

The qualitative behavior of both datasets in Fig. 2 reflects the dependence of the observed E-S efficiency on the trap energies of PSI and PSII. The photosynthetic trap energy is the energy at which the photochemical reaction occurs and energy is stored. The distribution of trap levels is expected to be narrow, as only one (or a pair of) molecule(s) is involved. Because there are two photosystems, with the PSII trap lying at a shorter wavelength than that of PSI ($\lambda_{t,II} < \lambda_{t,I}$), the traps are expected to define three spectral regimes of the overall efficiency, as long as the trap efficiencies differ. In Regime 1 (R1), where the excitation wavelength (λ_{ex}) is shorter (energy is greater) than that of either trap ($\lambda_{ex} < \lambda_{t,II} < \lambda_{t,I}$), captured excitations are transferred downhill to both reaction centers (excess energy is lost as heat), and both photosystems contribute to energy storage. The efficiency as measured by PA is therefore expected to decrease proportionally with decreasing wavelength.

In R2, excitation wavelengths are longer than that of the PSII trap, but shorter than that of the PSI trap ($\lambda_{t,II} < \lambda_{ex} < \lambda_{t,I}$); both photosystems contribute to storage, but storage by PSII is expected to decrease with increasing λ_{ex} because reaction at the trap energy requires uphill energy transfer, and thus has a barrier to the rate-determining process. It is possible to 'borrow' this energy from the heat bath and so cool the solution (which has been observed in special cases); however, the barrier results in an exponential slowing of the reaction. This slowing will decrease the efficiency of PSII by allowing more reverse and side reactions to occur (see the factor r in Eq. (A.3)). We note the present model does not allow for energy transfer from PSII to PSI in R2.

In R3, excitation wavelengths are longer than that of either trap ($\lambda_{t,II} < \lambda_{t,I} < \lambda_{ex}$), so both require uphill energy transfer to initiate photochemistry, and the efficiencies of both PSI and PSII are expected to decrease exponentially with increasing wavelength.

Consistent with these expectations, the observed efficiencies of both species in Fig. 2 are seen at short wavelengths ($\lambda < \approx 720$ nm

in *A. marina*, $\lambda < \approx 700$ nm in *S. leopoliensis*) to increase with increasing wavelength, and at long wavelengths ($\lambda > \approx 740$ nm in *Am*, $\lambda > \approx 700$ nm in *Sl*) to decrease continually with increasing wavelength from their maximal values, as expected for regions R1 and R3. The increase in efficiency in R1 is greater than expected from the ratio of trap to excitation energies because of the difference in efficiencies of the photosystems. Additionally, the drop in efficiency near 725 nm in *A. marina*, followed by a rise to the maximum, is consistent with the behavior expected for R2; *i.e.*, rapid loss of contributions by PSII to the observed efficiency, and continuing gain in contributions by PSI. A slight dip near 680 nm in *S. leopoliensis* is at the noise level. The observed decrease of efficiency with increasing wavelength in R3 was used to constrain the fits that determined the specific efficiencies and absolute trap energies of PSI and PSII in both *Am* and *Sl* (Appendix).

4.3. Modeling results

The fit results demonstrate Eq. (A.3) is able to provide an accurate quantitative description of the measured efficiencies. The observed and fitted values of λ_t in both species (Table 2) agree with previously reported values [15,38,41], and those of ε_t are consistent with the corresponding qualitative behaviors described above. Values of $\lambda_{t;I,II}$ approximately coincide with the observed local maxima at 720 and 735 nm in *A. marina*, and at 690 nm in *S. leopoliensis* (the apparent maximum at 675 nm is within the noise), and thus indicate the three anticipated spectral regimes.

4.3.1. Spectral region R1: $\lambda_{ex} < \lambda_{t,II} < \lambda_{t,I}$

The results shown in Table 2 indicate that R1 in *A. marina* lies approximately between 670 and 723 nm; *i.e.*, the shortest experimental wavelength and the best-constrained value of $\lambda_{t,II}$. Spectral regions R1 and R2 are not well differentiated in *S. leopoliensis* (uncertainties in $\lambda_{t,II}$ and $\lambda_{t,I}$ are ± 6 and ± 10 nm, respectively). The shortest wavelength-absorbing accessory pigments contributing to the present results in both cyanobacteria are phycobilins (absorption bands near 650 nm in *A. marina* and 630 nm in *S. leopoliensis* [Fig. 3, Table 1]). The best fits to the observed efficiency (Eq. (A.3)) were obtained when the phycobilin contributions to PSI, p_I, were 0 ± 0.1 in *Am* and 0.5 ± 0.1 in *Sl*. These results suggest phycobilins contribute only to storage by PSII in *Am*, but contribute in equal measure to both photosystems in *Sl* (see Eqs. (A.5)–(A.8)). This reflects known differences in the structural organization of phycobiliproteins between *A. marina* and other cyanobacteria; *e.g.*, the former utilizes phycobilin rods (PBP complexes) in light-harvesting [42], but does not manufacture phycobilisomes [4]. One *A. marina* strain, CCMEE 5410, lacks phycobiliproteins altogether [7,8]. We note that some evidence for energy transfer from biliproteins to PSI in *Am* has been reported [43]. PA measurements and analyses of the E-S efficiency in CCMEE 5410 and other strains would provide additional insight into the role of phycobilins in energy storage.

4.3.2. Spectral region R2: $\lambda_{t,II} < \lambda_{ex} < \lambda_{t,I}$

Table 2 indicates spectral region R2 lies between $\lambda_{t,II} \approx 723$ nm and $\lambda_{t,I} \approx 740$ nm in *A. marina* and between $\lambda_{t,II} \approx 671$ nm and $\lambda_{t,I} \approx 695$ nm in *S. leopoliensis*. The result $\lambda_{t,II} = 723 \pm 3$ nm in *Am* was obtained by fitting to the efficiency data with the fractional contributions to overall storage—$F_{I,II}$ in Eqs. (A.1)–(A.4)—determined by six underlying absorption bands (dashed curve in Fig. 2). This fit improves upon that obtained with $F_{I,II}$ determined by only three bands (solid curve), but only approximately captures the apparent dip in efficiency near 725 nm. Additional measurements would better-define the efficiency in this region, perhaps allowing a better fit with the current model. However, of note is that the presence of the PSII band near 716 nm and PSI band near 728 nm (Table 1, Column 2) leads to a crossing of the respective absorbance functions f_{II} and f_I (Eqs. (A.7) and (A.8)) near 725 nm, with f_{II} decreasing more rapidly than f_I (see circled feature in Fig. 3A). This

suggests that accurately modeling the observed dip may require specific components of PSI and PSII absorption that produce this crossing very precisely. In general, the model would benefit from expressions for $F_{I,II}$ obtained directly from data, without *a priori* assumptions about locations or shapes of underlying components. Further development of the model is in progress.

The result that $\lambda_{t,II}$ in *A. marina* lies near 723 nm agrees with evidence that the primary donor (trap) initiating photochemistry in PSII of *Am* is a Chl *d* accessory chlorophyll (Chl$_{D1}$) with site energy corresponding to a 724-nm photon, rather than the active-branch special-pair chlorophyll (P$_{D1}$) [15,17]. This is consistent with evidence that also in Chl *a* systems primary transfer initiates from an excited state localized at Chl$_{D1}$ rather than P$_{D1}$ [44–46]. In *A. marina*, the proposed scenario based on spectroscopic evidence [15,16] and theoretical analysis [17] is that downhill energy transfer from the predominantly Chl *d*-containing light-harvesting apparatus to the RC leads to excitation (near 724 nm) of a chlorophyll *d* at the Chl$_{D1}$ site, producing the state P$_{D1}$Chl$^*_{D1}$Pheo$_{D1}$. Electron transfer to the primary acceptor pheophytin *a* at the Pheo$_{D1}$ site then occurs: P$_{D1}$Chl$^*_{D1}$Pheo$_{D1}$ → P$_{D1}$Chl$^+_{D1}$Pheo$^-_{D1}$. Finally, Chl$^+_{D1}$ oxidizes P$_{D1}$, yielding the charge-separated state P$^+_{D1}$Chl$_{D1}$Pheo$^-_{D1}$, which ultimately oxidizes the OEC (Y$_Z$). The matter of whether P$_{D1}$ in *A. marina* is chlorophyll *a* or *d* has not been settled; however, that P$_{D1}$ is the primary electron-donor [20] is not supported by the present results.

Structural comparison of PSII in *A. marina* with that in the Chl *a* species, *T. elongatus*, indicates that the photosystem is highly conserved. The amino acid sequences of the respective core proteins are 85% (D1) and 88% (D2) identical [4,47]. Comparison of a homology model of the 3-D structure of D1/D2 in *A. marina* with a corresponding experimental *T. elongatus* structure [47] indicates that the only mutation in *Am* with the potential to influence primary photochemistry is the substitution Phe119→Tyr119 proximal to the accessory chlorophyll Chl$_{D1}$ [M. Dong, M. R. Gunner; personal communication]. When this pigment is Chl *d* in the model structure, the substitution enables hydrogen-bonding between the Tyr hydroxyl and Chl formyl moieties, suggesting a scenario in which *A. marina* has adapted the PSII RC specifically to ensure that the trap from which photochemistry initiates is a chlorophyll *d* molecule at Chl$_{D1}$.

In *S. leopoliensis*, a slight drop in efficiency at $\lambda_{ex} > \lambda_{t,II}$ (near 675 nm), followed by a rise to $\lambda_{t,I} \approx 695$ nm, is evident in the data but as stated previously is within the noise. Efforts in progress include repeating spectrally-dependent PA measurements for both species in the presence of the PSII and PSI inhibitors DCMU and DBMIB.

4.3.3. Spectral region R3: $\lambda_{t,II} < \lambda_{t,I} < \lambda_{ex}$

As noted above, the observed thermodynamic drop in efficiency in R3 in both *Am* and *Sl* (Fig. 2) provides a key constraint on the model because it unequivocally indicates the location of the PSI trap. Our results show that the overall efficiency is significant even at the longest flash wavelengths used [725 nm (*Sl*) and 760 nm (*Am*)], indicating that uphill energy transfer to both traps makes a significant contribution to energy storage.

Evidence of the decrease of quantum yield at long wavelengths has a long history, beginning with the observation of the Emerson enhancement effect in 1943 [48]. The explanation as the interaction of two separate photosystems is one of the milestones of photosynthesis research, but the expected decrease of yield at the longest wavelengths beyond those of both traps has been hard to document (*e.g.*, [49,50]). Most of the difficulty is in the determination of a small light absorption in a scattering medium. The photoacoustic methodology sidesteps this difficulty by measuring *only* the absorbed light and thus directly measures the energy-storage efficiency. It is limited only by the inevitable signal from the supporting or cellular material. This advantage is available because the efficiency is obtained from a ratio of signals at a given wavelength, where only the effect resulting from the absorbed photons is measured (Sections 2.2 and 3.1). The only requirement is that the sample absorption does not change between measurement in the dark and under saturating light (Section 2.2). Thus, the latter must be controlled to avoid heating, and the exciting light must have a well-defined wavelength distribution to avoid the trivial possibility of excitation by short wavelengths at the high energies often used ($\sim$mJ/cm^2). Previous measurements often employed filters of 10–20 nm bandwidth and so cannot be used for quantitative analysis. The current measurements, on the other hand, with 1-nm (0.002 eV) resolution and only 1% error in the signal, are well conditioned for such analysis.

There are claims [51] that the lower yield at long wavelengths is caused by the known [52] dependence of oxygen formation on the square of the intensity at very low intensities, because of the loss from the finite lifetimes of the S-states. However, the present measurements involve energy, not products, and are linear at the energies and rates employed (Fig. 1).

The data of Thapper et al. [53], which was obtained using a well-defined light source, documents the fact that all the effects of PSII, including oxygen formation, can be observed in spinach out to 780 nm. Even though the absolute yields were not determined, one can infer that the yield at 790 nm was <1%, which is in agreement with our data. We note that our finding of the absolute yield decrease in R3 allows a straightforward explanation of the results reported in Thapper et al. [53], without recourse to hypothesized new states of Chl, *etc.* Only uphill energy transfer is required.

Boichenko et al. [43] reported the action spectra of PSI and PSII in *A. marina*. However, comparison of the present results with their data is not possible at longer wavelengths, where we see large changes in efficiency but the action spectra are too weak to resolve.

4.3.4. PSI and PSII efficiencies at the trap wavelength

The E-S efficiencies at the trap wavelengths in *Am* ($\varepsilon_{t,I} = 43 \pm 2\%$, $\varepsilon_{t,II} = 32 \pm 1\%$) are comparable to those in *Sl* ($\varepsilon_{t,I} = 38 \pm 4\%$, $\varepsilon_{t,II} = 30 \pm 5\%$). The significant difference in PSI and PSII efficiencies gives a 'bias' to the observed efficiency and so contributes to the success of the model in isolating the contribution of each system. This difference agrees with previous data on *Chlorella* [27] and *Synechocystis* [54–56]. We note that the total efficiency at the trap wavelength must include losses associated with the primary reaction, and thus is given by $\varepsilon_{t,TOT} = \Phi \times \varepsilon_t$ [see Eq. (A.3)]. For the best fits to the PA data, $r^{-1} = 0.02 \Rightarrow \Phi = 98\%$, in which case the differences between $\varepsilon_{t,TOT}$ and ε_t are within the uncertainties of the latter.

4.4. Implications: the red limit of oxygenic photosynthesis

A significant adaptation enabling far-red oxygenic photosynthesis in *A. marina*, beyond utilization of Chl *d* for light harvesting, has been the incorporation of Chl *d* in both PSI and PSII reaction centers. This has preserved the efficiency of energy storage both by circumventing losses that would otherwise occur during uphill transfer from Chl *d*-containing antenna complexes to Chl *a*-containing RCs, and, at least in the case of PSII, by simultaneously preserving the basic mechanism for primary charge separation used by Chl *a* organisms. The present results and additional evidence cited above suggest that a key component of the latter may have been ensuring (*via* a specific amino acid substitution) that the trapping molecule is a Chl *d* accessory chlorophyll (Chl$_{D1}$).

Thermodynamics require that there is a long-wavelength limit of oxygenic photosynthesis that constrains possible modifications of the two-photosystem paradigm to accommodate red photons [53,57]. At some set of wavelengths in the far-red/near-IR, low trap energies must adversely affect photochemistry. In traps with too low-energy initial states, subsequent forward electron-transfer is thermodynamically hindered by competition from back- and side-reactions. This

reduces the yield, making photochemistry inefficient and the organism non-viable.

The present results demonstrate that photochemistry in *A. marina* is not at this limit, indicating that oxygenic photosynthesis at even longer wavelengths is plausible. This is supported by the aforementioned discovery of a cyanobacterium containing Chl *f*, in which a methyl→formyl substitution in Chl *a* shifts the *in vivo* Q$_Y$ absorption maximum ≈5 nm further to the red than that of Chl *d* [9,10]. Of note is that current evidence suggests Chl *f* is present only in the light-harvesting apparatus of this organism [5]. Further investigation of efficiency and mechanisms of oxygenic photosynthesis in *A. marina* and other far-red light-utilizing species will likely provide insights into water-utilizing photochemistry that are of broad relevance.

Avenues for further research include: PA measurements of the E-S efficiency in whole cells treated with inhibitors, as well as studies of isolated and purified PSI and PSII complexes; Identification of the specific products of photochemistry by resolution of the possible long timescale (>3 ms) components; Assessment of differences in electron-transfer kinetics between *A. marina* and other cyanobacteria; Quantification of natural variability in energy storage due, *e.g.*, to differing growth conditions or culture strains. The availability of more accurate *in vivo* redox potentials from other workers, in conjunction with additional PA experiments, would help quantify the contribution of entropic processes such as proton gradients and ATP formation to overall energy storage. Intriguingly, enhanced utilization of such processes by *A. marina* may be a mechanism by which it has adapted to its unique light environment.

5. Conclusions

We have presented PA measurements of the energy-storage efficiency of *in vivo* photosynthesis in two cyanobacteria over a 90-nm range of excitation wavelengths in the red region. These measurements are of unprecedented accuracy (1% error) and spectral resolution (1 nm), allowing the first detailed analysis of the spectral dependence of energy storage. Since PA measures the enthalpy of photochemistry, the present results provide the first direct observation of the photosystem trap energies.

Our conclusions are as follows: (1) The maximum observed E-S efficiency in *A. marina* (40 ± 1% at 735 nm) exceeds that in *S. leopoliensis* (35 ± 0.6% at 690 nm). (2) The same occurs at wavelength of peak Chl absorption, where in *Am* the efficiency is 36 ± 1% at 710 nm, and in *Sl* it is 31 ± 0.7% at 670 nm. (3) The E-S efficiency in *Am* at both trap wavelengths (32% at 723 nm [PSII], 43% at 740 nm [PSI]) again exceeds that in *Sl* (30% at 671 nm [PSII], 38% at 695 nm [PSI]). (4) Both trap wavelengths in *Am* are ≈40 nm longer than the corresponding wavelengths in *Sl*, and agree with previous results within the errors [15,41]; however, the present results are based directly on energy measurements, rather than inferred from spectroscopy. The PSII trap wavelength in *Am*, ≈723 nm, agrees with the suggestion of a 724-nm site energy for Chl$_{D1}$; *i.e.*, the primary donor is a Chl *d* molecule at the accessory site [16–18]. This result is also consistent with the suggestion that a Phe→Tyr substitution engenders hydrogen-bonding with Chl$_{D1}$ when it is Chl *d*. (5) The dip in efficiency at 725 nm evident in *Am* is not well-captured by the present model, possibly indicating omitted components of absorption. (6) In both species, the rate of decay of efficiency at wavelengths longer than that of either trap (spectral region R3) indicates that uphill energy transfer contributes significantly to overall storage.

Acknowledgements

Appendix A. Details of spectral efficiency model and analysis

Quantitative description of the *in vivo* energy-storage efficiency of oxygenic photosynthesis must account for the individual contributions of PSI and PSII to overall storage. The PA data from both *A. marina* and *S. leopoliensis* were therefore modeled using the expression:

$$\varepsilon_{obs}(\lambda) = F_I(\lambda)\varepsilon_I(\lambda) + F_{II}(\lambda)\varepsilon_{II}(\lambda). \tag{A.1}$$

Here, ε_{obs} is the observed E-S efficiency, $\varepsilon_{I,II}$ are the efficiencies specific to PSI and PSII, and $F_{I,II}$ weight the latter according to their fractional contributions to overall energy storage at a chosen excitation wavelength, which depend on the relative number and absorption cross-sections of the two photosystems (see below). Expanding $\varepsilon_{I,II}$ and omitting the notation for wavelength-dependence λ, Eq. (A.1) can be rewritten as:

$$\varepsilon_{obs} = F_I \frac{E_{t,I}}{E_{ex}} \Phi_I \varepsilon_{t,I} + F_{II} \frac{E_{t,II}}{E_{ex}} \Phi_{II} \varepsilon_{t,II}. \tag{A.2}$$

In Eq. (A.2), $E_{t;I,II} = hc/\lambda_{t;I,II}$ are the photon energies at the PSI and PSII trap wavelengths, $\lambda_{t;I,II}$; $E_{ex} = hc/\lambda_{ex}$ is the photon energy at the excitation wavelength, λ_{ex} (*i.e.*, the laser pulse wavelength at which the sample is excited); $\varepsilon_{t;I,II}$ are the E-S trap efficiencies of the two photosystems at $\lambda_{t;I,II}$; and $\Phi_{I,II}$ are the primary yields at $\lambda_{t;I,II}$. It is assumed that $\varepsilon_{t;I,II}$ are constants intrinsically determined by the respective photochemistries of PSI and PSII; and that the PQ pool circumvents the possibility of deficient electron flow between the photosystems that might otherwise affect ε_t. The ratios $E_{t;I,II}/E_{ex}$ account for the linear increase or decrease in observed efficiency, relative to ε_t, expected from decay of E_{ex} to E_t when $\lambda_{ex} < \lambda_t$, or from uphill transfer of E_{ex} to E_t when $\lambda_{ex} > \lambda_t$ (Section 2.3).

The trap yields $\Phi_{I,II}$ are equal to $r_{I,II}/(r_{I,II} + 1)$, where r, specific to each photosystem, is the ratio k_f/k_r; k_f is the forward rate constant for forming the primary ions; and k_r is the reverse (or other loss) rate constant. To allow for thermally-driven uphill energy transfer when $\lambda_{ex} > \lambda_t$, Φ for both traps was expressed as $sr/(sr + 1)$, where s is a factor exponentially slowing the forward reactions for decreasing $E_{ex} < E_t$ ($\lambda_{ex} > \lambda_t$): $s_{I,II} = \exp(-(E_{t;I,II} - E_{ex})/kT)$, where $kT_{293K} = 0.025$ eV. Thus, for $\lambda_{ex} > \lambda_t$, $s \to 0 \Rightarrow \Phi \to 0$; and for $\lambda_{ex} < \lambda_t$, $s \to \infty \Rightarrow \Phi \to 1$. Expressing $\Phi_{I,II}$, Eq. (A.2) becomes:

$$\varepsilon_{obs} = F_I \frac{E_{t,I}}{E_{ex}} \left(r_I^{-1} \exp\left[\frac{E_{t,I} - E_{ex}}{kT}\right] + 1 \right)^{-1} \varepsilon_{t,I} + F_{II} \frac{E_{t,II}}{E_{ex}} \left(r_{II}^{-1} \exp\left[\frac{E_{t,II} - E_{ex}}{kT}\right] + 1 \right)^{-1} \varepsilon_{t,II}. \tag{A.3}$$

The fractional contributions to energy storage, F_I and $F_{II} = 1 - F_I$, are determined by the fraction of photons absorbed by PSI or PSII, and thus reflect both the number and λ-dependent (effective) optical cross-sections of the photosystems. $F_{I,II}$ were written in terms of Gaussian absorption bands specific to PSI and/or PSII:

$$F_I = f_I/(f_I + f_{II}), \quad F_{II} = f_{II}/(f_I + f_{II}). \tag{A.4}$$

The Gaussian functions $f_{I,II}(\lambda)$ were determined by curve-fitting known PSI and PSII pigment bands to absorbance spectra obtained directly from the whole-cell samples used in the PA experiments (Section 2.1 and Section 3.3.1).

Our procedure for fitting Eq. (A.3) to the observed E-S efficiencies for *A. marina* and *S. leopoliensis* was as follows:

1) Obtain the photosystem-specific fractional contributions to the observed efficiency, $F_{I,II}$, from experimental absorbance data. Set

$p_I = 0$; *i.e.*, initially assume absorption by phycobilins contributes only to storage by PSII (see below and Section 4.3.1).

2) Set the ratios of rate constants $r_{I,II}^{-1}$ at fixed values corresponding to known primary yields, $\Phi_{I,II} = 1/(r_{I,II}^{-1} + 1)$. Initially, $\Phi_I = \Phi_{II} = 0.87 \Rightarrow r_I^{-1} = r_{II}^{-1} = 0.15$.

3) Set the PSI trap energy $E_{t,I}$ (*i.e.*, corresponding wavelength $\lambda_{t,I}$) at a fixed value within the observed range: 730 nm $< \lambda_{t,I} <$ 745 nm (*Am*), 685 nm $< \lambda_{t,I} <$ 705 nm (*Sl*). Initially, $\lambda_{t,I} =$ 730 nm (*Am*) or $\lambda_{t,I} =$ 685 nm (*Sl*).

4) With the three parameters $\lambda_{t,II}$, $\varepsilon_{t;I,II}$ free, fit Eq. (A.3) to the efficiency data.

5) Repeat Step 4 with other fixed values of $\lambda_{t,I}$ within the observed range until the fit with least RMS error is obtained.

6) With $\lambda_{t,I}$ fixed at the best value obtained in Step 5, repeat Step 4 with other fixed values of $r_{I,II}^{-1}$ corresponding to primary yields within the known range ($0.9 < \Phi_{I,II} < 1$) until the fit meeting the following criteria is obtained:
   (a) 700 nm $< \lambda_{t,II} <$ 730 nm (*Am*), 670 nm $< \lambda_{t,II} <$ 685 nm (*Sl*); AND
   (b) Least RMS error; AND (c) Smallest uncertainties in fitted values of the free parameters

7) With $r_{I,II}^{-1}$ fixed at best values obtained in Step 6, repeat Step 4 with other fixed values of $0 \le p_I \le 1$, until the fit meeting criteria (a)–(c) is obtained.

We next describe this procedure in detail.

A.1. Step 1: Fractional contributions to energy storage, $F_{I,II}(\lambda)$, from sample absorbance

A.1.1. A. marina (3 or 6 absorption bands)

The Gaussian functions $f_{I,II}(\lambda)$ in Eq. (A.4) were determined by curve-fitting to absorbance spectra from whole-cell samples used in the PA measurements (Section 2.1, Fig. 3). Fits were obtained by considering three or six absorption bands. For *A. marina*, inspection of Fig. 3A (filled circles) indicates at least two Chl *d* bands: a main band centered near 713 nm, and a shoulder near 695 nm. A band near 650 nm, associated with phycobilins [32,43,58], is also evident. In the case of three bands fit to the sample absorbance, the 713-nm band (*B*) was assigned to PSI, the 695-nm band (*H*) to PSII, and the 650-nm band (*E*) apportioned between PSI and PSII. The functions $f_{I,II}$ were therefore written as

$$f_I(\lambda) = A \exp\left(-(\lambda - B)^2 / 2C^2\right) + p_I D \exp\left(-(\lambda - E)^2 / 2F^2\right) \quad \text{(A.5)}$$

$$f_{II}(\lambda) = (1 - p_I) D \exp\left(-(\lambda - E)^2 / 2F^2\right) + G \exp\left(-(\lambda - H)^2 / 2I^2\right). \quad \text{(A.6)}$$

Here, $0 \le p_I \le 1$ denotes the fractional contribution of phycobilins associated with PSI. The sum $f_I + f_{II}$ was fit to the absorbance data (solid curve in Fig. 3A) to obtain the set of parameters *A*, *B*, *C*, *D*, *E*, *F*, *G*, *H*, and *I* (Table 1, first column [Section 3.3.1]). Fitting was carried out by nonlinear least-squares using MATLAB [29] with initial parameter values chosen from inspection of the data.

A more detailed consideration of the λ-dependent contributions of the photosystems ($F_{I,II}$) improves fits of Eq. (A.3) to the efficiency data (see below and Section 3.3.2). Inclusion of longer-wavelength absorption bands may allow PSII to contribute to the observed energy storage even at $\lambda \approx 740$ nm in *A. marina*. Studies employing whole cells [32,43,58] or isolated complexes [19,59,60] at cryogenic or room temperatures have indicated additional PSI bands at least near 728 and 740 nm, and additional PSII bands at least near 715 nm. We expanded Eqs. (A.5) and (A.6) to include these contributions:

$$f_I(\lambda) = A \exp\left(-(\lambda - B)^2 / 2C^2\right) + p_I D \exp\left(-(\lambda - E)^2 / 2F^2\right)$$
$$+ J \exp\left(-(\lambda - K)^2 / 2L^2\right) + M \exp\left(-(\lambda - N)^2 / 2O^2\right) \quad \text{(A.7)}$$

$$f_{II}(\lambda) = (1 - p_I) D \exp\left(-(\lambda - E)^2 / 2F^2\right) + G \exp\left(-(\lambda - H)^2 / 2I^2\right)$$
$$+ P \exp\left(-(\lambda - Q)^2 / 2R^2\right). \quad \text{(A.8)}$$

Here, bands centered at *B*, *E*, and *H* are the same bands near 713, 650, and 695 nm as in Eqs. (A.5) and (A.6), and p_I is again the fraction of phycobilin absorption associated with PSI. In Eqs. (A.7) and (A.8), bands centered at *K*, *N*, and *Q* were assigned as PSI bands near 728 and 740 nm, and a PSII band near 715 nm, respectively. The sum Eq. (A.7) + Eq. (A.8) was fit by inspection to the *A. marina* absorbance data to obtain the set of parameters *A*–*R* that minimizes the RMSE (Table 1, second column [Section 3.3.1]). We note that spectroscopic information is inherently variable, differing, *e.g.*, between isolated complexes and whole cells, and between room-temperature and cryogenic conditions.

A.1.2. S. leopoliensis (3 absorption bands)

For *S. leopoliensis*, inspection of Fig. 3B (open circles) indicates at least two Chl *a* bands: a main band centered near 670 nm, and a shoulder near 685 nm. A phycobilin band near 625 nm is also present (peak not shown). Fits of Eq. (A.3) to the PA results for *S. leopoliensis* were obtained by first fitting these three bands (Eq. (A.5) + Eq. (A.6)) to the sample absorbance spectrum (solid curve in Fig. 3B), with initial parameter values chosen from inspection of the data. The 685-nm band (*B*) was assigned to PSI, the 670-nm band (*H*) to PSII, and the 625-nm band (*E*) apportioned between PSI and PSII.

One best fit of Eq. (A.3) to the PA results was obtained for each of the three $F_{I,II}$ derived from the absorption fits just described—one fit to the *A. marina* efficiency data assuming three underlying bands; one fit to the *Am* data assuming six bands; and one fit to the *Sl* data assuming three bands. Because the absorption fits are well-constrained by experimental information (*e.g.*, low RMS error), both from the same samples used in the PA measurements and from the literature, the parameters in Eqs. (A.5)–(A.8) were considered determined for purposes of the efficiency fits, and therefore did not introduce degrees of freedom. However, as discussed below, the accuracy of the fits was sensitive to the choice of underlying absorption bands in $F_{I,II}$. Initially, it was assumed the phycobilin bands contribute only to storage by PSII [$p_I = 0$ in Eqs. (A.5)–(A.8)]. The three fits of Eq. (A.3) to the PA results (Fig. 2) were carried out as follows.

A.2. Steps 2–7: PSI and PSII trap wavelengths ($\lambda_{t;I,II}$) and E-S efficiencies ($\varepsilon_{t;I,II}$) from PA data

A.2.1. A. marina (3 or 6 absorption bands)

With $F_{I,II}(\lambda)$ determined by sample absorption, $r_{I,II}^{-1}$ initially set at 0.15 (corresponding to $\Phi_{I,II} = 0.87$), and p_I initially set at 0 (Steps 1–2), Eq. (A.3) was fit to the E-S efficiency results for fixed trial values of $\lambda_{t,I}$ constrained by the data to lie within the range 730 nm $< \lambda_{t,I} <$ 745 nm (Steps 3–5). In this spectral region, the measured efficiency is observed to be maximal, and beyond this region it is observed to decrease continually to its minimum value (Fig. 2). As discussed in Section 4.2, this behavior unequivocally identifies $\lambda_{t,I}$, because at longer wavelengths ($\lambda > \lambda_{t,I}$) excitation of either trap requires uphill energy transfer with exponentially decreasing efficiency. For each fixed value of $\lambda_{t,I}$, the three remaining parameters—$\lambda_{t,II}$, $\varepsilon_{t,I}$, and $\varepsilon_{t,II}$—were fit to the efficiency data by nonlinear least-squares until the result with least RMS error was obtained.

Next (Step 6), with $\lambda_{t,I}$ set at its best value from Steps 3–5, fits of $\lambda_{t,II}$, and $\varepsilon_{t;I,II}$ were performed with r_I^{-1} and r_{II}^{-1} fixed at values between 0.15 and 0.01 (corresponding to primary yields within the known range, $0.87 < \Phi_{I,II} < 0.99$ [21,61]) until the following criteria were simultaneously met: (a) 700 nm $< \lambda_{t,II} <$ 730 nm; (b) least RMS error; and (c) least uncertainty in final values of $\lambda_{t,II}$, $\varepsilon_{t;I,II}$. The PSII

trap must lie at a wavelength both shorter than that of the PSI trap (<730 nm) and consistent with absorption by Chl d (>700 nm). Finally (Step 7), with $r_{I,II}^{-1}$ set at their best values from Step 6, $\lambda_{t,II}$, $\varepsilon_{t;I,II}$ were again fit with p_I fixed at values between 0 and 1 until criteria (a)–(c) were satisfied. Uncertainties in the fixed parameters were estimated by refitting them to the data with the remaining parameters fixed at their best-fit values.

A.2.2. S. leopoliensis (3 absorption bands)

As in *A. marina*, except the ranges for $\lambda_{t,I}$ and $\lambda_{t,II}$ are constrained by the data (Fig. 2) to be 685 nm$<\lambda_{t,I}<705$ nm and 670 nm$<\lambda_{t,II}<685$ nm.

References

[1] D. Mauzerall, Why chlorophyll? Ann. N. Y. Acad. Sci. 206 (1973) 483–494.
[2] D. Mauzerall, Chlorophyll and photosynthesis, Philos. Trans. R. Soc. Lond. C 273 (1976) 287–294.
[3] L. Björn, G.C. Papageorgiou, R.E. Blankenship, Govindjee, A viewpoint: why chlorophyll a? Photosynth. Res. 99 (2009) 85–98.
[4] W.D. Swingley, M. Chen, P.C. Cheung, A.L. Conrad, L.C. Dejesa, J. Hao, B.M. Honchak, L.E. Karbach, A. Kurdoglu, S. Lahiri, S.D. Mastrian, H. Miyashita, L. Page, P. Ramakrishna, S. Satoh, W.M. Sattley, Y. Shimada, H.L. Taylor, T. Tomo, T. Tsuchiya, Z.T. Wang, J. Raymond, M. Mimuro, R.E. Blankenship, J.W. Touchman, Niche adaptation and genome expansion in the chlorophyll d-producing cyanobacterium *Acarylochloris marina*, Proc. Natl. Acad. Sci. U. S. A. 105 (2008) 2005–2010.
[5] M. Chen, R.E. Blankenship, Expanding the solar spectrum used by photosynthesis, Trends Plant Sci. 16 (2011) 427–431.
[6] H. Miyashita, H. Ikemoto, N. Kurano, K. Adachi, M. Chihara, S. Miyachi, Chlorophyll d as a major pigment, Nature 383 (1996) 402.
[7] S.R. Miller, S. Augustine, T. Le Olson, R.E. Blankenship, J. Selker, A.M. Wood, Discovery of a free-living chlorophyll d-producing cyanobacterium with a hybrid proteobacterial/cyanobacterial small-subunit rRNA gene, Proc. Natl. Acad. Sci. U. S. A. 102 (2005) 850–855.
[8] S.R. Miller, A.M. Wood, R.E. Blankenship, M. Kim, S. Ferriera, Dynamics of gene duplication in the genomes of chlorophyll d-producing cyanobacteria: implications for the ecological niche, Genome Biol. Evol. 3 (2011) 601–613.
[9] M. Chen, M. Schliep, R.D. Willows, Z.L. Cai, B.A. Neilan, H. Scheer, A red-shifted chlorophyll, Science 329 (2010) 1318–1319.
[10] M. Chen, Y. Li, D. Birch, R.D. Willows, A cyanobacterium that contains chlorophyll f — a red-absorbing photopigment, FEBS Lett. 586 (2012) 3249–3254.
[11] S. Lopez-Legentil, B. Song, M. Bosch, J.R. Pawlik, X. Turon, Cyanobacterial diversity and a new *Acarychloris*-like symbiont from Bahamian sea-squirts, PLoS One 6 (2011) 12.
[12] T. Tomo, S.I. Allakhverdiev, M. Mimuro, Constitution and energetics of photosystem I and photosystem II in the chlorophyll d-dominated cyanobacterium *Acaryochloris marina*, J. Photochem. Photobiol. B 104 (2011) 333–340.
[13] M. Kobayashi, S. Ohashi, K. Iwamoto, Y. Shiraiwa, Y. Kato, T. Watanabe, Redox potential of chlorophyll d in vitro, Biochim. Biophys. Acta Bioenerg. 1767 (2007) 596–602.
[14] T. Tomo, Y. Kato, T. Suzuki, S. Akimoto, T. Okubo, T. Noguchi, K. Hasegawa, T. Tsuchiya, K. Tanaka, M. Fukuya, N. Dohmae, T. Watanabe, M. Mimuro, Characterization of highly purified photosystem I complexes from the chlorophyll d-dominated cyanobacterium *Acaryochloris marina* MBIC 11017, J. Biol. Chem. 283 (2008) 18198–18209.
[15] E. Schlodder, M. Cetin, H.J. Eckert, F.J. Schmitt, J. Barber, A. Telfer, Both chlorophylls a and d are essential for the photochemistry in photosystem II of the cyanobacteria, *Acaryochloris marina*, Biochim. Biophys. Acta Bioenerg. 1767 (2007) 589–595.
[16] K. Cser, Z. Deak, A. Telfer, J. Barber, I. Vass, Energetics of Photosystem II charge recombination in *Acaryochloris marina* studied by thermoluminescence and flash-induced chlorophyll fluorescence measurements, Photosynth. Res. 98 (2008) 131–140.
[17] T. Renger, E. Schlodder, The primary electron donor of photosystem II of the cyanobacterium *Acaryochloris marina* is a chlorophyll d and the water oxidation is driven by a chlorophyll a/chlorophyll d heterodimer, J. Phys. Chem. B 112 (2008) 7351–7354.
[18] T. Renger, E. Schlodder, Primary photophysical processes in photosystem II: bridging the gap between crystal structure and optical spectra, Chemphyschem 11 (2010) 1141–1153.
[19] T. Tomo, T. Okubo, S. Akimoto, M. Yokono, H. Miyashita, T. Tsuchiya, T. Noguchi, M. Mimuro, Identification of the special pair of photosystem II in a chlorophyll d-dominated cyanobacterium, Proc. Natl. Acad. Sci. U. S. A. 104 (2007) 7283–7288.
[20] S.I. Allakhverdiev, T. Tomo, Y. Shimada, H. Kindo, R. Nagao, V.V. Klimov, M. Mimuro, Redox potential of pheophytin a in photosystem II of two cyanobacteria having the different special pair chlorophylls, Proc. Natl. Acad. Sci. U. S. A. 107 (2010) 3924–3929.
[21] H. Dau, I. Zaharieva, Principles, efficiency, and blueprint character of solar-energy conversion in photosynthetic water oxidation, Acc. Chem. Res. 42 (2009) 1861–1870.
[22] R.E. Blankenship, D.M. Tiede, J. Barber, G.W. Brudvig, G. Fleming, M. Ghirardi, M.R. Gunner, W. Junge, D.M. Kramer, A. Melis, T.A. Moore, C.C. Moser, D.G. Nocera, A.J. Nozik, D.R. Ort, W.W. Parson, R.C. Prince, R.T. Sayre, Comparing photosynthetic and photovoltaic efficiencies and recognizing the potential for improvement, Science 332 (2011) 805–809.
[23] S. Malkin, D. Cahen, Photoacoustic spectroscopy and radiant energy conversion: theory of the effect with special emphasis on photosynthesis, Photochem. Photobiol. 29 (1979) 803–813.
[24] D.C. Fork, S.K. Herbert, The application of photoacoustic techniques to studies of photosynthesis, Photochem. Photobiol. 57 (1993) 207–220.
[25] T. Gensch, C. Viappiani, Time-resolved photothermal methods: accessing time-resolved thermodynamics of photoinduced processes in chemistry and biology, Photochem. Photobiol. Sci. 2 (2003) 699–721.
[26] S.P. Mielke, N.Y. Kiang, R.E. Blankenship, M.R. Gunner, D. Mauzerall, Efficiency of photosynthesis in a Chl d-utilizing cyanobacterium is comparable to or higher than that in Chl a-utilizing oxygenic species, Biochim. Biophys. Acta 1807 (2011) 1231–1236.
[27] Y. Cha, D.C. Mauzerall, Energy storage of linear and cyclic electron flows in photosynthesis, Plant Physiol. 100 (1992) 1869–1877.
[28] D.C. Mauzerall, Determination of oxygen emission and uptake in leaves by pulsed, time resolved photoacoustics, Plant Physiol. 94 (1990) 278–283.
[29] The MathWorks, Inc., Natick, MA, v. R2011b.
[30] D. Charlebois, D. Mauzerall, Energy storage and optical cross-section of PS I in the cyanobacterium *Synechococcus* PCC 7002 and a psaE$^-$ mutant, Photosynth. Res. 59 (1999) 27–38.
[31] R. Krivanek, H. Dau, M. Haumann, Enthalpy changes during photosynthetic water oxidation tracked by time-resolved calorimetry using a photothermal beam deflection technique, Biophys. J. 94 (2008) 1890–1903.
[32] H. Schiller, H. Senger, H. Miyashita, S. Miyachi, H. Dau, Light-harvesting in *Acaryochloris marina* — spectroscopic characterization of a chlorophyll d-dominated photosynthetic antenna system, FEBS Lett. 410 (1997) 433–436.
[33] D.J. Lundell, A.N. Glazer, A. Melis, R. Malkin, Characterization of a cyanobacterial photosystem I complex, J. Biol. Chem. 260 (1985) 646–654.
[34] M. Yang, A. Damjanovic, H.M. Vaswani, G.R. Fleming, Energy transfer in photosystem I of cyanobacteria *Synechococcus elongatus*: model study with structure-based semi-empirical Hamiltonian and experimental spectral density, Biophys. J. 85 (2003) 140–158.
[35] J. Nield, O. Kruse, J. Ruprecht, P. da Fonseca, C. Buchel, J. Barber, Three-dimensional structure of *Chlamydomonas reinhardtii* and *Synechococcus elongatus* photosystem II complexes allows for comparison of their oxygen-evolving complex organization, J. Biol. Chem. 275 (2000) 27940–27946.
[36] R.D. Britt, in: D.R. Ort, C.F. Yocum (Eds.), Oxygenic Photosynthesis: The Light Reactions, Kluwer, Dordrecht, 1996, pp. 139–164.
[37] N. Cassan, B. Lagoutte, P. Setif, Ferredoxin-NADP$^+$ reductase. Kinetics of electron transfer, transient intermediates, and catalytic activities studied by flash-absorption spectroscopy with isolated photosystem I and ferredoxin, J. Biol. Chem. 280 (2005) 25960–25972.
[38] R.E. Blankenship, Molecular Mechanisms of Photosynthesis, Blackwell, Oxford, 2002.
[39] G. Bernát, M. Rögner, Center of the cyanobacterial electron transport network: the cytochrome b6f complex, in: G.A. Peschek, C. Obinger, G. Renger (Eds.), The Bioenergetic Processes in Cyanobacteria – from Evolutionary Singularity to Ecological Diversity, Springer, Dordrecht, 2011, pp. 573–606.
[40] S.P. Mielke, D. Mauzerall, Energy changes in photosynthetic electron transport: Probing photosynthesis by pulsed photoacoustics, in: J.H. Golbeck, A.v.d. Est (Eds.) The Biophysics of Photosynthesis, submitted for publication.
[41] Q. Hu, H. Miyashita, I. Iwasaki, N. Kurano, S. Miyachi, M. Iwaki, S. Itoh, A photosystem I reaction center driven by chlorophyll d in oxygenic photosynthesis, Proc. Natl. Acad. Sci. U. S. A. 95 (1998) 13319–13323.
[42] J. Marquardt, H. Senger, H. Miyashita, S. Miyachi, E. Morschel, Isolation and characterization of biliprotein aggregates from *Acaryochloris marina*, a Prochloron-like prokaryote containing mainly chlorophyll d, FEBS Lett. 410 (1997) 428–432.
[43] V.A. Boichenko, V.V. Klimov, H. Miyashita, S. Miyachi, Functional characteristics of chlorophyll d-predominating photosynthetic apparatus in intact cells of *Acaryochloris marina*, Photosynth. Res. 65 (2000) 269–277.
[44] B.A. Diner, F. Rappaport, Structure, dynamics, and energetics of the primary photochemistry of photosystem II of oxygenic photosynthesis, Annu. Rev. Plant Biol. 53 (2002) 551–580.
[45] G. Raszewski, W. Saenger, T. Renger, Theory of optical spectra of photosystem II reaction centers: location of the triplet state and the identity of the primary electron donor, Biophys. J. 88 (2005) 986–998.
[46] G. Raszewski, B.A. Diner, E. Schlodder, T. Renger, Spectroscopic properties of reaction center pigments in photosystem II core complexes: revision of the multimer model, Biophys. J. 95 (2008) 105–119.
[47] A. Guskov, J. Kern, A. Gabdulkhakov, M. Broser, A. Zouni, W. Saenger, Cyanobacterial photosystem II at 2.9-A resolution and the role of quinones, lipids, channels and chloride, Nat. Struct. Mol. Biol. 16 (2009) 334–342.
[48] R. Emerson, C.M. Lewis, The dependence of the quantum yield of *Chlorella* photosynthesis on wavelength of light, Am. J. Bot. 30 (1943) 165–178.
[49] C. Wilhelm, T. Jakob, Uphill energy transfer from long-wavelength absorbing chlorophylls to PS II in *Ostreobium* sp. is functional in carbon assimilation, Photosynth. Res. 87 (2006) 323–329.
[50] H.-W. Trissl, Long-wavelength absorbing antenna pigments and heterogeneous absorption bands concentrate excitons and increase absorption cross section, Photosynth. Res. 35 (1993) 247–263.
[51] Y. Zeinalov, L. Maslenkova, On the action spectra of photosynthesis and spectral dependence of the quantum efficiency, Bulg. J. Plant Physiol. 26 (2000) 58–69.

[52] B. Diner, D. Mauzerall, Feedback controlling oxygen production in a cross-reaction between two photosystems in photosynthesis, Biochim. Biophys. Acta 305 (1973) 329–352.

[53] A. Thapper, F. Mamedov, F. Mokvist, L. Hammarstrom, S. Styring, Defining the far-red limit of photosystem II in spinach, Plant Cell 21 (2009) 2391–2401.

[54] J.M. Hou, V.A. Boichenko, Y.C. Wang, P.R. Chitnis, D. Mauzerall, Thermodynamics of electron transfer in oxygenic photosynthetic reaction centers: a pulsed photoacoustic study of electron transfer in photosystem I reveals a similarity to bacterial reaction centers in both volume change and entropy, Biochemistry 40 (2001) 7109–7116.

[55] J.M. Hou, V.A. Boichenko, B.A. Diner, D. Mauzerall, Thermodynamics of electron transfer in oxygenic photosynthetic reaction centers: volume change, enthalpy, and entropy of electron-transfer reactions in manganese-depleted photosystem II core complexes, Biochemistry 40 (2001) 7117–7125.

[56] V.A. Boichenko, J.M. Hou, D. Mauzerall, Thermodynamics of electron transfer in oxygenic photosynthetic reaction centers: volume change, enthalpy, and entropy

of electron-transfer reactions in the intact cells of the cyanobacterium *Synechocystis* PCC 6803, Biochemistry 40 (2001) 7126–7132.

[57] H. Pettai, V. Oja, A. Freiberg, A. Laisk, The long-wavelength limit of plant photosynthesis, FEBS Lett. 579 (2005) 4017–4019.

[58] M. Chen, R.G. Quinnell, A.W.D. Larkum, Chlorophyll d as the major photopigment in *Acaryochloris marina*, J. Porphyrins Phthalocyanines 6 (2002) 763–773.

[59] M. Chen, A. Telfer, S. Lin, A. Pascal, A.W. Larkum, J. Barber, R.E. Blankenship, The nature of the photosystem II reaction centre in the chlorophyll d-containing prokaryote, *Acaryochloris marina*, Photochem. Photobiol. Sci. 4 (2005) 1060–1064.

[60] M. Mimuro, T. Tomo, T. Tsuchiya, Two unique cyanobacteria lead to a traceable approach of the first appearance of oxygenic photosynthesis, Photosynth. Res. 97 (2008) 167–176.

[61] M. Byrdin, P. Jordan, N. Krauss, P. Fromme, D. Stehlik, E. Schlodder, Light harvesting in photosystem I: modeling based on the 2.5-A structure of photosystem I from *Synechococcus elongatus*, Biophys. J. 83 (2002) 433–457.